J|A|C|S ARTICLES

Published on Web 09/15/2010

Structure and Bonding of Isoleptic Coinage Metal (Cu, Ag, Au) Dimethylaminonitrenes in the Gas Phase

Alexey Fedorov,[†] Erik P. A. Couzijn,[†] Natalia S. Nagornova,[‡] Oleg V. Boyarkin,*[,‡] Thomas R. Rizzo,[‡] and Peter Chen*[,†]

Laboratorium für Organische Chemie, ETH Zürich, Wolfgang-Pauli-Strasse 10, CH-8093 Zürich, Switzerland, and Laboratoire de Chimie Physique Moléculaire, École Polytechnique Fédérale de Lausanne, CH-1015 Lausanne, Switzerland

Received June 8, 2010; E-mail: peter.chen@org.chem.ethz.ch; oleg.boiarkin@epfl.ch

Abstract: Dimethylaminonitrene complexes of $IMesM^+$ (IMes =1,3-bis(2,4,6-trimethylphenyl)imidazol-2-ylidene; M = Cu, Ag, Au) were prepared in the gas phase and structurally characterized by high-resolution infrared spectroscopy of the cold species, ion−molecule reactions, and DFT computations. We measured the binding energies of the nitrene fragment to the $IMesM^+$ moiety by energy-resolved collision-induced dissociation experiments in the gas phase, affording a trend in bond strength of M = Cu ≈ Au > Ag. This trend is explained in terms of a detailed metal−nitrogen bonding analysis, from which relativistic effects on the bonding were assessed. Various density functionals were evaluated for reproducing the observed thermochemical data and Truhlar's M06 functional was found to give the best agreement.

Introduction

In the last two decades, the detection and manipulation of reactive metal−organic intermediates *via* electrospray-ionization tandem mass spectrometry (ESI-MS/MS) has become widely practiced.[1] "Ion fishing" to extract reactive intermediates from solution by ESI-MS became popular because of (1) its very high sensitivity as compared to other methods; (2) its high (mass-) selectivity; and (3) the ability to use ESI-MS for online monitoring, thus allowing the detection of such species despite their usually low concentration during a reaction. Tandem MS has deepened our understanding of metal-catalyzed hydrogenation,[2] C−H activation,[3] olefin metathesis,[4] Ziegler−Natta zirconocene polymerization,[5] aldehyde olefination,[6] ethene polymerization with palladium catalysis,[7] transmetalation,[8] phosphinidine cycloaddition,[9] and reductive elimination,[10] among other processes.

The recent tremendous surge in interest in gold-catalyzed reactions[11] has begged the question of which bonding interactions occur in gold complexes and how these interactions differ (or not) from those in the analogous copper and silver complexes. Our recent reports of the targeted synthesis and reactions of gold carbenes[12] in the gas phase has opened the way to systematically study the bonding in different series of complexes that are closely related to catalytic species, for which

[†] ETH Zürich.
[‡] École Polytechnique Fédérale de Lausanne.

(1) (a) Chen, P. *Angew. Chem., Int. Ed.* **2003**, *42*, 2832–2847. (b) Plattner, D. A. *Int. J. Mass Spectrom.* **2001**, *207*, 125–144. (c) Plattner, D. A. *Top. Curr. Chem.* **2003**, *225*, 153–203. (d) Santos, L. S.; Knaack, L.; Metzger, J. O. *Int. J. Mass Spectrom.* **2005**, *246*, 84–104. (e) O'Hair, R. A. J. *Chem. Commun.* **2006**, 1469–1481. (f) Eberlin, M. N. *Eur. J. Mass Spectrom.* **2007**, *13*, 19–28. (g) Tureček, F. *Mass Spectrom. Rev.* **2007**, *26*, 563–582. (h) Santos, L. S. *Eur. J. Org. Chem.* **2008**, 235–253. (i) Chisholm, D. M.; McIndoe, J. S. *Dalton Trans.* **2008**, 3933–3945. (j) Roithová, J.; Schröder, D. *Coord. Chem. Rev.* **2009**, *253*, 666–677. (k) Müller, C. A.; Markert, C.; Teichert, A. M.; Pfaltz, A. *Chem. Commun.* **2009**, 1607–1618. (l) Colton, R.; D'Agostino, A.; Traeger, J. C. *Mass Spectrom. Rev.* **1995**, *14*, 79–106.

(2) (a) Kim, Y.-M.; Chen, P. *Int. J. Mass Spectrom.* **1999**, *185*−*187*, 871–881. (b) Hartmann, R.; Chen, P. *Angew. Chem., Int. Ed.* **2001**, *40*, 3581–3585. (c) Dietiker, R.; Chen, P. *Angew. Chem., Int. Ed.* **2004**, *43*, 5513–5516.

(3) (a) Hinderling, C.; Feichtinger, D.; Plattner, D. A.; Chen, P. *J. Am. Chem. Soc.* **1997**, *119*, 10793–10804. (b) Hinderling, C.; Plattner, D. A.; Chen, P. *Angew. Chem., Int. Ed.* **1997**, *36*, 243–244. (c) Gerdes, G.; Chen, P. *Organometallics* **2003**, *22*, 2217–2225. (d) Gerdes, G.; Chen, P. *Organometallics* **2004**, *23*, 3031–3036. (e) Hammad, L. A.; Gerdes, G.; Chen, P. *Organometallics* **2005**, *24*, 1907–1913. (f) Moret, M.-E.; Chen, P. *Organometallics* **2007**, *26*, 1523–1530. (g) Moret, M.-E.; Chen, P. *J. Am. Chem. Soc.* **2009**, *131*, 5675–5690.

(4) (a) Hinderling, C.; Adlhart, C.; Chen, P. *Angew. Chem., Int. Ed.* **1998**, *37*, 2685–2689. (b) Adlhart, C.; Volland, M. A. O.; Hofmann, P.; Chen, P. *Helv. Chim. Acta* **2000**, *83*, 3306–3311. (c) Adlhart, C.; Chen, P. *Helv. Chim. Acta* **2000**, *83*, 2192–2196. (d) Adlhart, C.; Hinderling, C.; Baumann, H.; Chen, P. *J. Am. Chem. Soc.* **2000**, *122*, 8204–8214. (e) Volland, M. A. O.; Adlhart, C.; Kiener, C. A.; Chen, P.; Hofmann, P. *Chem.*−*Eur. J.* **2001**, *7*, 4621–4632. (f) Chen, X.; Zhang, X.; Chen, P. *Angew. Chem., Int. Ed.* **2003**, *42*, 3798–3801. (g) Zhang, X.; Chen, X.; Chen, P. *Organometallics* **2004**, *23*, 3437–3447. (h) Frech, C. M.; Blacque, O.; Schmalle, H. W.; Berke, H.; Adlhart, C.; Chen, P. *Chem.*−*Eur. J.* **2006**, *12*, 3325–3338. (i) Torker, S.; Merki, D.; Chen, P. *J. Am. Chem. Soc.* **2008**, *130*, 4808–4814.

(5) (a) Feichtinger, D.; Plattner, D. A.; Chen, P. *J. Am. Chem. Soc.* **1998**, *120*, 7125–7126. (b) di Lena, F.; Quintanilla, E.; Chen, P. *Chem. Commun.* **2005**, 5757–5759. (c) Quintanilla, E.; di Lena, F.; Chen, P. *Chem. Commun.* **2006**, 4309–4311. (d) Dietiker, R.; di Lena, F.; Chen, P. *J. Am. Chem. Soc.* **2007**, *129*, 2796–2802. (e) di Lena, F.; Chen, P. *Helv. Chim. Acta* **2009**, *92*, 890–896.

(6) Zhang, X.; Chen, P. *Chem.*−*Eur. J.* **2003**, *9*, 1852–1859.

(7) (a) Hinderling, C.; Chen, P. *Angew. Chem., Int. Ed.* **1999**, *38*, 2253–2256. (b) Hinderling, C.; Chen, P. *Int. J. Mass Spectrom.* **2000**, *195*−*196*, 377–383.

(8) Moret, M.-E.; Serra, D.; Bach, A.; Chen, P. *Angew. Chem., Int. Ed.* **2010**, *49*, 2873–2877.

(9) Jansen, H.; Samuels, M. C.; Couzijn, E. P. A.; Slootweg, J. C.; Ehlers, A. W.; Chen, P.; Lammertsma, K. *Chem.*−*Eur. J.* **2010**, *16*, 1454–1458.

(10) Couzijn, E. P. A.; Zocher, E.; Bach, A.; Chen, P. *Chem.*−*Eur. J.* **2010**, *16*, 5408–5415.

the ligand sphere is constant but the metal is varied within group 11. To address the central question of bonding across the isoleptic series of copper, silver, and gold[13] aminonitrene complexes, we employ two families of experimental physical techniques alongside quantum chemical calculations. Computational methods do address the question for copper, silver, and gold but nevertheless show great need of benchmarking and verification.

Gas-phase studies of the characteristic reactivity of such complexes and, in particular, kinetic experiments such as energy-resolved threshold collision-induced dissociation (T-CID) measurements[14] can provide the information required for a comparison with theoretical calculations.[3e,f,4i,8,10,12a,13,15] For increasingly complicated systems the nature of the reacting species may no longer be unambiguously deducible from the T-CID results alone, and one needs to employ complementary structure-sensitive methods for a reliable assignment. High-resolution infrared spectroscopy measures a specific "fingerprint" pattern (frequencies, widths, intensities) of vibrational transitions in a molecule and therefore provides a stringent test for theory and greatly facilitates selection of the most likely structure among those suggested by calculations.[16]

Resolution becomes a crucial issue for spectroscopy of large molecules with complicated vibrational structures, such as organometallic complexes. Infrared multiphoton dissociation (IRMPD) by a free electron laser (FEL) has been employed for vibrational spectroscopy of several organometallic intermediates.[17,18] However, such experiments often leave a large ambiguity in selecting the true structure of the studied ions. This uncertainty is mainly due to low spectral resolution,[19] which originates from spectral congestion in room temperature measurements and, to some extent, from the broad bandwidth of FELs. In addition, FELs do not operate efficiently in the region of 2500−3700 cm^{-1}, where many characteristic light-atom stretch vibrations absorb. Moreover, the fact that IRMPD relies on a multiphoton process makes direct comparison with calculated data questionable[20] in contrast to single-photon, linear absorption spectra. Instead, in this work, we use a widely tunable midresolution optical parametric oscillator (OPO) and extensive cooling of the sample ions to perform vibrationally resolved linear IR spectroscopy,[16c,d] based on a change of UV photodissociation yield upon IR pre-excitation. While being readily applied to biomolecules,[16] acquisition of highly resolved spectra of organometallic reactive intermediates has yet to become widely practiced.[21]

Here we report on the intrinsic features of Cu, Ag, and Au aminonitrene complexes as revealed by a combination of gas-phase ion−molecule reactions and computational analyses, which demonstrate the importance of relativistic effects for the bonding in the gold complex. The identity of these species within the isoleptic series is confirmed through a comparison of calculated vibrational spectra with the measured highly resolved infrared spectra of the cold ions in the gas phase.

Methods

General. Phosphazene adducts **2**-Cu and **2**-Ag were prepared as described earlier for **2**-Au[13] (Scheme 1) and utilized *in situ* due to their solution-state lability and, for **2s**-Ag, light sensitivity.[22]

Threshold CID Measurements. Mass spectrometric measurements were performed on a Finnigan MAT TSQ-700 instrument

(11) (a) Zhang, L.; Sun, J.; Kozmin, S. A. *Adv. Synth. Catal.* **2006**, *348*, 2271–2296. (b) Hashmi, A. S. K.; Hutchings, G. J. *Angew. Chem., Int. Ed.* **2006**, *45*, 7896–7936. (c) Fürstner, A.; Davies, P. W. *Angew. Chem., Int. Ed.* **2007**, *46*, 3410–3449. (d) Gorin, D. J.; Toste, F. D. *Nature* **2007**, *446*, 395–403. (e) Jiménez-Núñez, E.; Echavarren, A. M. *Chem. Commun.* **2007**, 333–346. (f) Hashmi, A. S. K. *Chem. Rev.* **2007**, *107*, 3180–3211. (g) Yamamoto, Y. *J. Org. Chem.* **2007**, *72*, 7817–7831. (h) Muzart, J. *Tetrahedron* **2008**, *64*, 5815–5849. (i) Kirsch, S. F. *Synthesis* **2008**, *20*, 3183–3204. (j) Li, Z.; Brouwer, C.; He, C. *Chem. Rev.* **2008**, *108*, 3239–3265. (k) Arcadi, A. *Chem. Rev.* **2008**, *108*, 3266–3325. (l) Jiménez-Núñez, E.; Echavarren, A. M. *Chem. Rev.* **2008**, *108*, 3326–3350. (m) Gorin, D. J.; Sherry, B. D.; Toste, F. D. *Chem. Rev.* **2008**, *108*, 3351–3378. (n) Patil, N. T.; Yamamoto, Y. *Chem. Rev.* **2008**, *108*, 3395–3442. (o) Widenhoefer, R. A. *Chem.—Eur. J.* **2008**, *14*, 5382–5391. (p) Michelet, V.; Toullec, P. Y.; Genêt, J.-P. *Angew. Chem., Int. Ed.* **2008**, *47*, 4268–4315. (q) Soriano, E.; Marco-Contelles, J. *Acc. Chem. Res.* **2009**, *42*, 1026–1036.

(12) (a) Fedorov, A.; Moret, M.-E.; Chen, P. *J. Am. Chem. Soc.* **2008**, *130*, 8880–8881. (b) Fedorov, A.; Chen, P. *Organometallics* **2009**, *28*, 1278–1281. (c) Batiste, L.; Fedorov, A.; Chen, P. *Chem. Commun.* **2010**, *46*, 3899–3901. (d) Fedorov, A.; Chen, P. *Organometallics* **2010**, *29*, 2994–3000.

(13) Fedorov, A.; Batiste, L.; Couzijn, E. P. A.; Chen, P. *ChemPhysChem* **2010**, *11*, 1002–1005.

(14) (a) Armentrout, P. B. *Top. Curr. Chem.* **2003**, *225*, 233–262. (b) Armentrout, P. B. *Acc. Chem. Res.* **1995**, *28*, 430–436. (c) Rodgers, M. T.; Ervin, K. M.; Armentrout, P. B. *J. Chem. Phys.* **1997**, *106*, 4499–4508. (d) Rodgers, M. T.; Armentrout, P. B. *Mass Spectrom. Rev.* **2000**, *19*, 215–247. (e) Armentrout, P. B. *Annu. Rev. Phys. Chem.* **2001**, *52*, 423–461. (f) Armentrout, P. B.; Ervin, K. M.; Rodgers, M. T. *J. Phys. Chem. A* **2008**, *112*, 10071–10085.

(15) (a) Zocher, E.; Dietiker, R.; Chen, P. *J. Am. Chem. Soc.* **2007**, *129*, 2476–2481. (b) Zocher, E.; Sigrist, R.; Chen, P. *Inorg. Chem.* **2007**, *46*, 11366–11370.

(16) (a) Rizzo, T. R.; Stearns, J. A.; Boyarkin, O. V. *Int. Rev. Phys. Chem.* **2009**, *28*, 481–515. (b) Carney, J. R.; Zwier, T. S. *J. Phys. Chem. A* **2000**, *104*, 8677–8688. (c) Boyarkin, O. V.; Mercier, S. R.; Kamariotis, A.; Rizzo, T. R. *J. Am. Chem. Soc.* **2006**, *128*, 2816–2817. (d) Stearns, J. A.; Guidi, M.; Boyarkin, O. V.; Rizzo, T. R. *J. Chem. Phys.* **2007**, *127*, 154322–154327. (e) Stearns, J. A.; Mercier, S.; Seaiby, C.; Guidi, M.; Boyarkin, O. V.; Rizzo, T. R. *J. Am. Chem. Soc.* **2007**, *129*, 11814–11820. (f) Stearns, J. A.; Seaiby, C.; Boyarkin, O. V.; Rizzo, T. R. *Phys. Chem. Chem. Phys.* **2009**, *11*, 125–132. (g) Nagornova, N. S.; Rizzo, T. R.; Boyarkin, O. V. *J. Am. Chem. Soc.* **2010**, *132*, 4040–4041.

(17) MacAleese, L.; Maître, P. *Mass Spectrom. Rev.* **2007**, *26*, 583–605.

(18) For selected recent work, see: (a) Milko, P.; Roithová, J.; Schröder, D.; Lemaire, J.; Schwarz, H.; Holthausen, M. C. *Chem.—Eur. J.* **2008**, *14*, 4318–4327. (b) Milko, P.; Roithová, J.; Tsierkezos, N.; Schröder, D. *J. Am. Chem. Soc.* **2008**, *130*, 7186–7187. (c) Tyo, E. C.; Castleman, A. W.; Schröder, D.; Milko, P.; Roithová, J.; Ortega, J. M.; Cinellu, M. A.; Cocco, F.; Minghetti, G. *J. Am. Chem. Soc.* **2009**, *131*, 13009–13019. (d) Roithová, J.; Milko, P. *J. Am. Chem. Soc.* **2010**, *132*, 281–288.

(19) (a) Lucas, B.; Grégoire, G.; Lemaire, J.; Maître, P.; Ortega, J. M.; Rupenyan, A.; Reimann, B.; Schermann, J. P.; Desfrançois, C. *Phys. Chem. Chem. Phys.* **2004**, *6*, 2659–2663. (b) Oomens, J.; Polfer, N.; Moore, D. T.; van der Meer, L.; Marshall, A. G.; Eyler, J. R.; Meijer, G.; von Helden, G. *Phys. Chem. Chem. Phys.* **2005**, *7*, 1345–1348. (c) Vaden, T. D.; Gowers, S. A. N.; de Boer, T. S. J. A.; Steill, J. D.; Oomens, J.; Snoek, L. C. *J. Am. Chem. Soc.* **2008**, *130*, 14640–14650.

(20) Kupser, P.; Pagel, K.; Oomens, J.; Polfer, N.; Koksch, B.; Meijer, G.; von Helden, G. *J. Am. Chem. Soc.* **2010**, *132*, 2085–2093.

(21) (a) Miller, M. E.; Grant, E. R. *J. Am. Chem. Soc.* **1987**, *109*, 7951–7960. (b) Weiller, B. H.; Grant, E. R. *J. Am. Chem. Soc.* **1987**, *109*, 1051–1055. (c) Weiller, B. H.; Grant, E. R. *J. Phys. Chem.* **1988**, *92*, 1458–1464. (d) Weitz, E. *J. Phys. Chem.* **1987**, *91*, 3945–3953. (e) House, P. G.; Weitz, E. *J. Phys. Chem. A* **1997**, *101*, 2988–2995. (f) van Heijnbergen, D.; von Helden, G.; Meijer, G.; Maître, P.; Duncan, M. A. *J. Am. Chem. Soc.* **2002**, *124*, 1562–1563. (g) Walters, R. S.; Pillai, E. D.; Schleyer, P. V.; Duncan, M. A. *J. Am. Chem. Soc.* **2005**, *127*, 17030–17042. (h) Citir, M.; Altinay, G.; Metz, R. B. *J. Phys. Chem. A* **2006**, *110*, 5051–5057. (i) Pillai, E. D.; Jaeger, T. D.; Duncan, M. A. *J. Am. Chem. Soc.* **2007**, *129*, 2297–2307. (j) Ricks, A. M.; Reed, Z. D.; Duncan, M. A. *J. Am. Chem. Soc.* **2009**, *131*, 9176–9177. (k) Altinay, G.; Citir, M.; Metz, R. B. *J. Phys. Chem. A* **2010**, *114*, 5104–5112.

(22) NMR spectra of the Cu and Ag silver phosphazene adducts **2** contain signals analogous to those of **2**-Au but the samples are contaminated by decomposition products. In the preparation of **2**-Ag analogous to ref 13, no silver triflate was added as this led to larger amounts of decomposition, presumably due to conproportionation.

Scheme 1. Synthesis and Gas-Phase Fragmentation of Isoleptic Adducts **2**-M

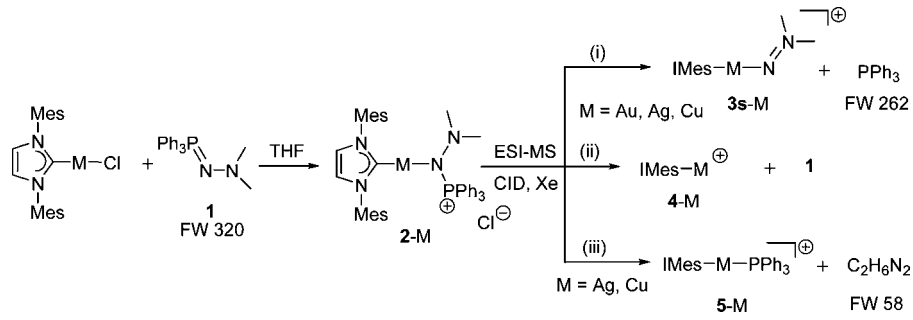

in which the first transfer octopole has been replaced by a custom-made 24-pole ion guide as described elsewhere.[10] Species of interest were introduced by electrospray ionization (ESI) of 0.1 mM solutions in dichloromethane and were mass-selected in the first quadrupole and collided with argon or xenon in the octopole collision cell to give characteristic fragmentation products, which were analyzed in the second quadrupole. The resolution for parent-ion selection was kept low ($m/\Delta m \approx 100$) to maintain a near-Gaussian ion kinetic energy distribution and optimal signal intensity, but high enough to ensure that the produced fragments originated only from the ions of interest.

For the threshold CID measurements,[10] three independent data sets were collected for each of the two dissociation processes studied. Reaction parameters and standard deviations were obtained from 15 fits with the program L-CID.[23] We assumed nine free rotors for **3s**-Cu and for **3s**-Ag: the eight methyl groups and the whole dimethylamino fragment. For the reaction barriers E_0 the standard deviations include a 0.15 eV laboratory-frame uncertainty.

Gas-Phase IR Spectroscopy. Details of the experimental setup for the IR measurements have been described elsewhere.[16c,d] Gas-phase ions were produced from 0.3 mM methanol solution at atmospheric pressure using nanoelectrospray. A glass capillary with metallized ends samples the nanospray plume and guides the ions into the vacuum chamber, where they are accumulated in a hexapole ion trap. After approximately 40 ms, the ions are released from the hexapole and passed through a quadrupole mass filter, which selects parent ions of a particular mass-to-charge ratio (m/z). An rf-only octopole guides them into a 22-pole ion trap, which is cooled to 6 K by a closed-cycle refrigerator (Sumitomo, SRDK-408). A pulse of helium, introduced into the trap before the arrival of the ion packet, collisionally cools the ions. We allow ~35 ms after this pulse for ion cooling and He pumping out before interrogating the ions with lasers. UV photofragmentation is performed using the 2−3 mJ output of a frequency-doubled dye laser pumped by 7 ns pulses of a Nd:YAG laser. Parent ions and the charged photofragments are released from the trap, guided through the second quadrupole mass filter (QMF-2) and collected on a channeltron. Monitoring the number of photofragment ion counts as a function of wavenumber of the UV laser generates a UV photofragmentation spectrum. For measurements of IR spectra we employ the IR−UV double resonance technique, where an IR pulse precedes the UV pulse by approximately 100 ns. IR absorption spectra of parent ions are generated by scanning the wavenumber of the IR laser while fixing the wavenumber of the UV laser on a photofragmentation transition, and monitoring the change of the fragmentation yield. Whenever the IR laser is in resonance with a vibrational transition of the parent ions, they absorb the light and become internally hot. Such vibrational heating results in a spectral broadening that may influence the subsequent UV photodissociation yield, usually depleting it. For IR spectroscopy in the 2800−3600 cm^{-1} region we use 5−6 mJ output of an optical parametric oscillator (OPO, LaserVision), pumped by a Nd:YAG laser. Pulses of 1−1.5 mJ in the 1400−1800 cm^{-1} spectral region were generated by difference frequency mixing 40 mJ of signal (~5500 cm^{-1}) and idler (~3800 cm^{-1}) waves, delivered by the same OPO, in an $AgGaSe_2$ crystal.

Density Functional Calculations. Geometry optimizations were performed with Gaussian09[24] at the M06/cc-pVDZ(-PP) level,[25,26] using tight geometry and SCF convergence criteria and an ultrafine integration grid. For species with a two-coordinate metal center, the redundant internal coordinates were modified; the angle and dihedrals involving the nearly linear metal−ligand bonds were removed, and a direct connection between the coordinating atoms of both ligands was built, which automatically adds also the related angles and dihedrals. Whereas the geometries were thus still fully optimized, this modification greatly reduced the number of cycles needed to reach convergence. Subsequent analytical frequency analyses were carried out to confirm the nature of each stationary point. However, despite their full optimization, species **14**-Cu and transition states $\mathbf{TS_{3s\text{-}14}}$-Cu and $\mathbf{TS_{11-12}}$-Cu featured a small imaginary frequency (of 15, 10, and 16 cm^{-1}, respectively) corresponding to rotation of a mesityl methyl group. For **14**-Cu the methyl group was rotated by steps of 15° in a linear transit calculation, which showed that the original structure was indeed the minimum. The rotational barrier is very small at ~0.04 kcal mol^{-1}, suggesting that the aforementioned spurious imaginary frequencies are due to numerical inaccuracies.

Energy decomposition analyses were conducted with the ADF suite[27] using the BP86/TZP density, treating relativistic effects with the scalar zeroth-order regular approximation and applying an integration accuracy of 6.0. The M−N bonds in coinage metal−nitrene complexes **3s**-M were analyzed in terms of the separate $IMesM^+$ cation and the singlet aminonitrene. The net bonding energy ΔE_{Net} consists of four contributions: the preparation energy ΔE_{prep} required to deform the fragments from their equilibrium structures to their geometries in the complex; the steric interactions between the fragments due to Pauli repulsion (ΔE_{Pauli}) and electrostatic attraction (ΔV_{elstat}); and the orbital interaction energy ΔE_{oi}. The use of M06/cc-pVDZ(-PP) geometries that were optimized with imposed C_s symmetry[28] enabled a further separation of ΔE_{oi} into mirror-symmetric (A′) and -antisymmetric (A″) contributions. The charge redistribution from $IMesM^+$ causes the orbital energy levels of both fragments to shift, complicating a detailed analysis of the individual

(23) Narancic, S.; Bach, A.; Chen, P. *J. Phys. Chem. A* **2007**, *111*, 7006–7013.

(24) Frisch, M. J.; et al. Gaussian 09, Revision A.02; Gaussian, Inc.: Wallingford, CT, 2009.

(25) (a) Zhao, Y.; Truhlar, D. G. *J. Chem. Phys.* **2006**, *125*, 194101. (b) Zhao, Y.; Truhlar, D. G. *Theor. Chem. Acc.* **2008**, *120*, 215–241. (c) Zhao, Y.; Truhlar, D. G. *Acc. Chem. Res.* **2008**, *41*, 157–167. (d) Cramer, C. J.; Truhlar, D. G. *Phys. Chem. Chem. Phys.* **2009**, *11*, 10757–10816.

(26) Figgen, D.; Rauhut, G.; Dolg, M.; Stoll, H. *Chem. Phys.* **2005**, *311*, 227–244.

(27) (a) *ADF2008.01, SCM, Theoretical Chemistry*;Vrije Universiteit: Amsterdam, The Netherlands. (b) te Velde, G.; Bickelhaupt, F. M.; van Gisbergen, S. J. A.; Fonseca Guerra, C.; Baerends, E. J.; Snijders, J. G.; Ziegler, T. *J. Comput. Chem.* **2001**, *22*, 931–967. (c) Fonseca Guerra, C.; Snijders, J. G.; te Velde, G.; Baerends, E. J. *Theor. Chem. Acc.* **1998**, *99*, 391–403.

fragment orbital interactions. Therefore, printouts were requested of the overlap matrix and the Fock matrix;[29] after the SCF, the diagonal elements of the latter correspond to the fragment orbital energies in the field of the total complex. Furthermore, the net amount of electron transfer between the fragments was assessed by their Hirshfeld charges.[30]

Energy evaluations for several density functionals were performed with ADF[27] using the BP86/TZP density, treating relativistic effects with the spin−orbit-coupled zeroth-order regular approximation. For assessment of the singlet−triplet energy gap for **3**-M spin isomers, the energy of the triplet species **3t**-M was calculated with the same method but using the noncollinear approximation for the spin polarization.

Results

The importance of relativistic effects in the bonding of cationic gold species[31] was first highlighted by Schwarz,[32] who reported that these account for more than 70% of the bond energy in $[AuCH_2]^+$. Whether contributions of this magnitude appear for larger, more articulated complexes, and whether these contributions are chemically significant for the burgeoning field of catalysis with gold complexes is an open question. A general, phenomenological resemblance of Cu and Au, as well as their distinction to Ag, begs for an explanation. For example, while *N*-heterocyclic carbene complexes of both Cu and Au prove effective in cyclopropanation[33] and induce similar reactions with alkynes as soft Lewis acids,[34] the related complexes of Ag mostly appear in the literature as transfer agents for the *N*-heterocyclic carbene ligand itself, a role in which the Ag complexes excel.[35]

We choose to study the aminonitrene complexes of Cu, Ag, and Au (**3s**-M, Scheme 1) for several reasons. On the practical side, metal nitrene complexes have been implied in catalytic aziridination and insertion reactions,[36] although the present aminonitrenes appear to be too strongly stabilized to engage in such a transformation.[13,37] On the theoretical side, bonding to the nitrene moiety should show both σ and π components, for which the changes going from Cu to Au may not be the same. Lastly, the aminonitrene complexes for all three metals in Group 11 are accessible via the same chemistry, display parallel fragmentation behavior albeit with different dissociation barriers, and can be shown to have analogous structures (*vide infra*).

CID of Isoleptic Phosphazene Adducts. We have previously reported that the IMes-supported phosphazene gold adduct **2**-Au can be easily prepared (Scheme 1) and detaches triphenylphosphine to furnish an interesting singlet aminonitrene species **3s**-Au upon ESI-MS and CID with argon.[13,38] With xenon as the collision gas, the more efficient energy transfer causes a second, more energetic channel to set in, corresponding to decoordination of the phosphazene ligand (Figure 1A). Remarkably, upon electrospray ionization, mass selection and CID with Xe, analogously prepared isoleptic copper and silver adducts **2** feature a third channel (Figures 1B, C and path (iii) in Scheme 1) that was not observed with any appreciable intensity for **2**-Au. The *m*/*z* ratio of the third fragmentation pathway identifies the unexpected exit channel as IMes-M-PPh_3^+ (M = Ag, Cu), which corresponds to loss of the aminonitrene (58 mass units) from the parent adduct. Threshold CID results for these systems are discussed in the Supporting Information.

Threshold CID Experiments. Similar to our previous reports on the gas-phase synthesis of gold benzylidenes[12] and **3s**-Au,[13] copper and silver aminonitrenes could be generated during the spray process by applying higher tube lens voltages to induce elimination of the PPh_3 protecting group in **2**-M.[39] Our assignment of the ion currents with *m*/*z* 425 and 470 (Figure 2) to metal-coordinated aminonitrenes is rationalized in detail below.

Gas-phase thermochemical data on the aminonitrene−metal binding in **3s**-Ag and **3s**-Cu were obtained by energy-resolved T-CID measurements (Figure 2).[10] The dimethylaminonitrene detachment was fitted with L-CID[23] using a loose transition-state model, i.e. assuming no activation barrier for the reverse reaction, which afforded a dissociation energy of 52.2 ± 1.3 kcal mol^{-1} for **3s**-Cu and of 46.5 ± 2.0 kcal mol^{-1} for the silver analogue (Figure 2B and D). We have reported previously[13] that rupture of the N−Au bond in **3s**-Au requires 50.7 ± 1.6 kcal mol^{-1}.

Having acquired experimental data on the M−N bond strengths in isoleptic aminonitrenes **3s**, we compared these values with theoretically predicted barriers as obtained with ADF for various density functionals (see Methods for details). For the arguments provided in the Supporting Information, we use Truhlar's M06 functional[25] to report dissociation energies for

(28) For silver and gold complexes **3s**-M the optimal geometries already have C_s symmetry, whereas the copper analogue is desymmetrized by a slight torsion of ~6.6° of the aminonitrene relative to the IMes moiety, amounting to a stabilization of merely 0.07 kcal mol^{-1}.

(29) Bickelhaupt, F. M.; Solà, M.; Fonseca Guerra, C. *J. Mol. Model.* **2006**, *12*, 563–568.
(30) Hirshfeld, F. L. *Theor. Chim. Acta* **1977**, *44*, 129–138.
(31) (a) Pyykkö, P. *Chem. Soc. Rev.* **2008**, *37*, 1967–1997. (b) Pyykkö, P. *Angew. Chem., Int. Ed.* **2004**, *43*, 4412–4456. (c) Pyykkö, P. *Angew. Chem., Int. Ed.* **2002**, *41*, 3573–3578. (d) Pyykkö, P. *Chem. Rev.* **1988**, *88*, 563–594. (e) Schwerdtfeger, P.; Boyd, P. D. W.; Burell, A. K.; Robinson, W. T.; Taylor, M. J. *Inorg. Chem.* **1990**, *29*, 3593–3607.
(32) Heinemann, C.; Hertwig, R. H.; Wesendrup, R.; Koch, W.; Schwarz, H. *J. Am. Chem. Soc.* **1995**, *117*, 495–500.
(33) (a) Fructos, M. R.; Belderrain, T. R.; de Frémont, P.; Scott, N. M.; Nolan, S. P.; Díaz-Requejo, M. M.; Pérez, P. J. *Angew. Chem., Int. Ed.* **2005**, *44*, 5284–5288. (b) Ricard, L.; Gagosz, F. *Organometallics* **2007**, *26*, 4704–4707. (c) Fañanás-Mastral, M.; Aznar, F. *Organometallics* **2009**, *28*, 666–668. (d) For cyclopropanation catalyzed by NHC silver complexes, see: Prieto, A.; Fructos, M. R.; Díaz-Requejo, M. M.; Pérez, P. J.; Pérez-Galán, P.; Delpont, N.; Echavarren, A. M. *Tetrahedron* **2009**, *65*, 1790–1793.
(34) (a) Patil, N. T.; Yamamoto, Y. *Chem. Rev.* **2008**, *108*, 3395–3442. (b) Naodovic, M.; Yamamoto, H. *Chem. Rev.* **2008**, *108*, 3132–3148, Also, see ref 11.
(35) (a) de Frémont, P.; Scott, N. M.; Stevens, E. D.; Nolan, S. P. *Organometallics* **2005**, *24*, 2411–2418. (b) Hahn, F. E.; Jahnke, M. C. *Angew. Chem., Int. Ed.* **2008**, *47*, 3122–3172. (c) Díez-González, S.; Marion, N.; Nolan, S. P. *Chem. Rev.* **2009**, *109*, 3612–3676. Also, see: (d) Belmont, P.; Parker, E. *Eur. J. Org. Chem.* **2009**, 6075–6089.
(36) (a) Müller, P.; Fruit, C. *Chem. Rev.* **2003**, *103*, 2905–2919. (b) Díaz-Requejo, M. M.; Pérez, P. J. *Chem. Rev.* **2008**, *108*, 3379–3394. (c) Sweeney, J. B. In *Aziridines and Epoxides in Organic Synthesis*; Yudin, A. K., Ed.; Wiley VCH: Weinheim, 2006; pp 117−144. (d) Collet, F.; Dodd, R. H.; Dauban, P. *Chem. Commun.* **2009**, 5061–5074.
(37) (a) Kuznetsov, M. A.; Ioffe, B. V. *Russ. Chem. Rev.* **1989**, *58*, 732–746. (b) Ioffe, B. V.; Kuznetsov, M. A. *Russ. Chem. Rev.* **1972**, *41*, 131–145. (c) Platz, M. S. In *Reactive Intermediate Chemistry*; Moss, R. A., Platz, M. S., Jones, M., Eds.; Wiley: Weinheim, 2004; pp 501−559. (d) Lemal, D. M. In *Nitrenes*; Lwowski, W., Ed.; Interscience: New York, 1970; Chapter 10. (e) Bock, H.; Dammel, R. *Angew. Chem., Int. Ed.* **1987**, *26*, 504–526.
(38) Throughout the manuscript a substance number followed by symbol "s" is used to indicate a corresponding singlet spin isomer. ADF BP86/TZP single-point calculations with the spin-orbit zeroth-order relativistic approximation yield singlet−triplet energy gaps of 19.3, 23.4, and 30.8 kcal mol^{-1} for **3**-Cu, **3**-Ag, and **3**-Au, respectively. These species are thus appropriately described as purely singlet complexes.
(39) For unmasking of reactive intermediates for MS studies, see: (a) Stevens, A. E.; Beauchamp, J. L. *J. Am. Chem. Soc.* **1978**, *100*, 2584–2585. (b) O'Hair, R. A. In *Reactive Intermediates*; Santos, L. S., Ed.; Wiley VCH: Weinheim, 2010; pp 199−227.

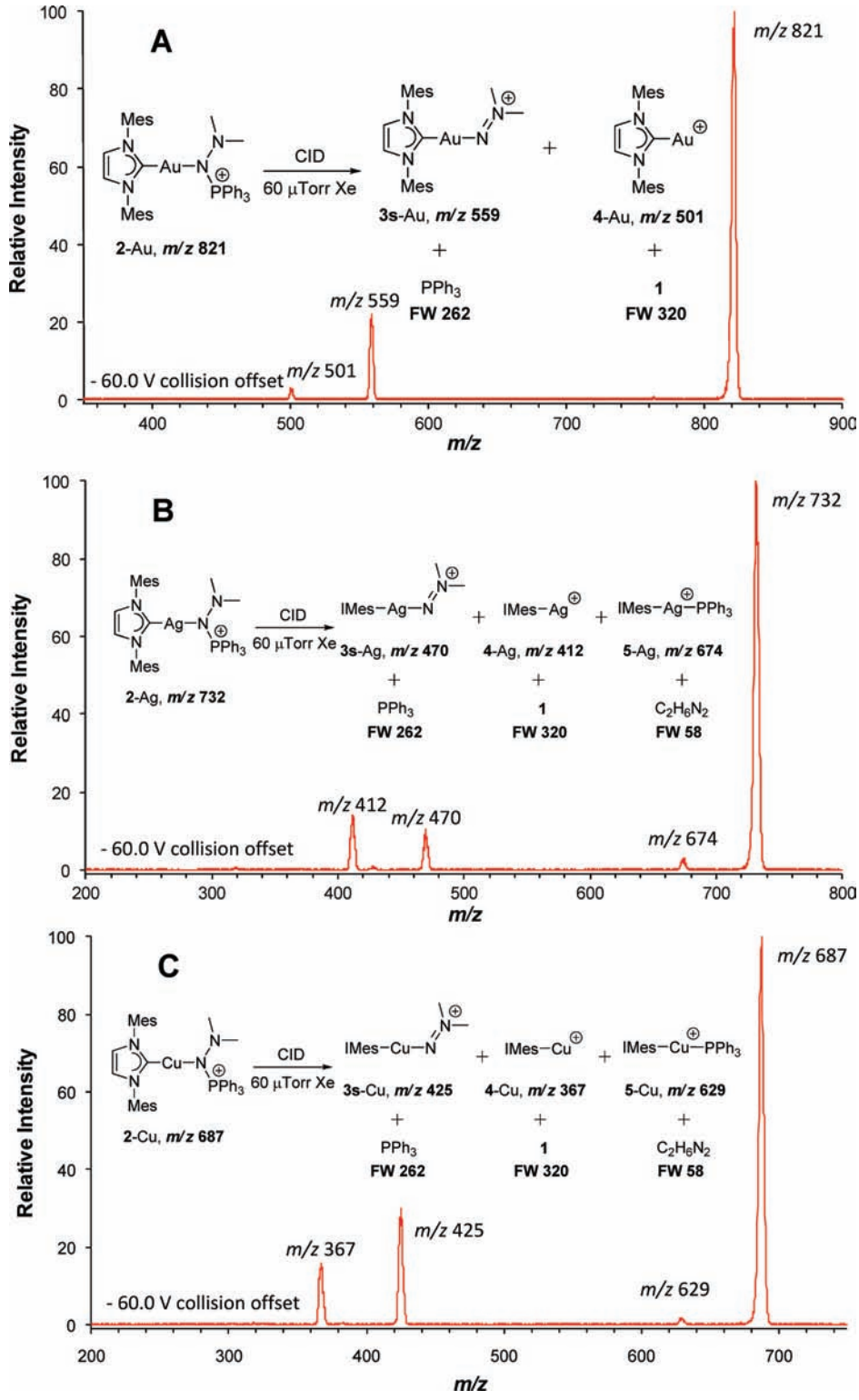

Figure 1. Daughter-ion spectra obtained after selection of cations **2**-M and CID with xenon in the octopole collision cell, demonstrating competing fragmentations.

the process **3s** → **4** + **6s** (Table 1). We also employed this method for the calculation of the potential energy surface for possible isomerization pathways of **3s** (*vide infra*).

Silver was argued by theoreticians to be the most "normal" metal among the coinage triad,[31b] whereas the computational treatment is complicated for copper due to strong electron−electron repulsion between its compact d orbitals, and for gold due to large relativistic effects.[31] One would therefore expect good agreement between experiment and theory for T-CID of **3s**-Ag, as is indeed obtained. While for silver the calculated aminonitrene dissociation energy is within the experimental error bars, the bond strengths for copper and gold are overestimated by ∼8 kcal mol^{-1} (Table 1).

Bonding Energy Decomposition Analyses. We performed computational energy decomposition analyses[27] of the M−N bond in aminonitrene complexes **3s** so as to explain the trend

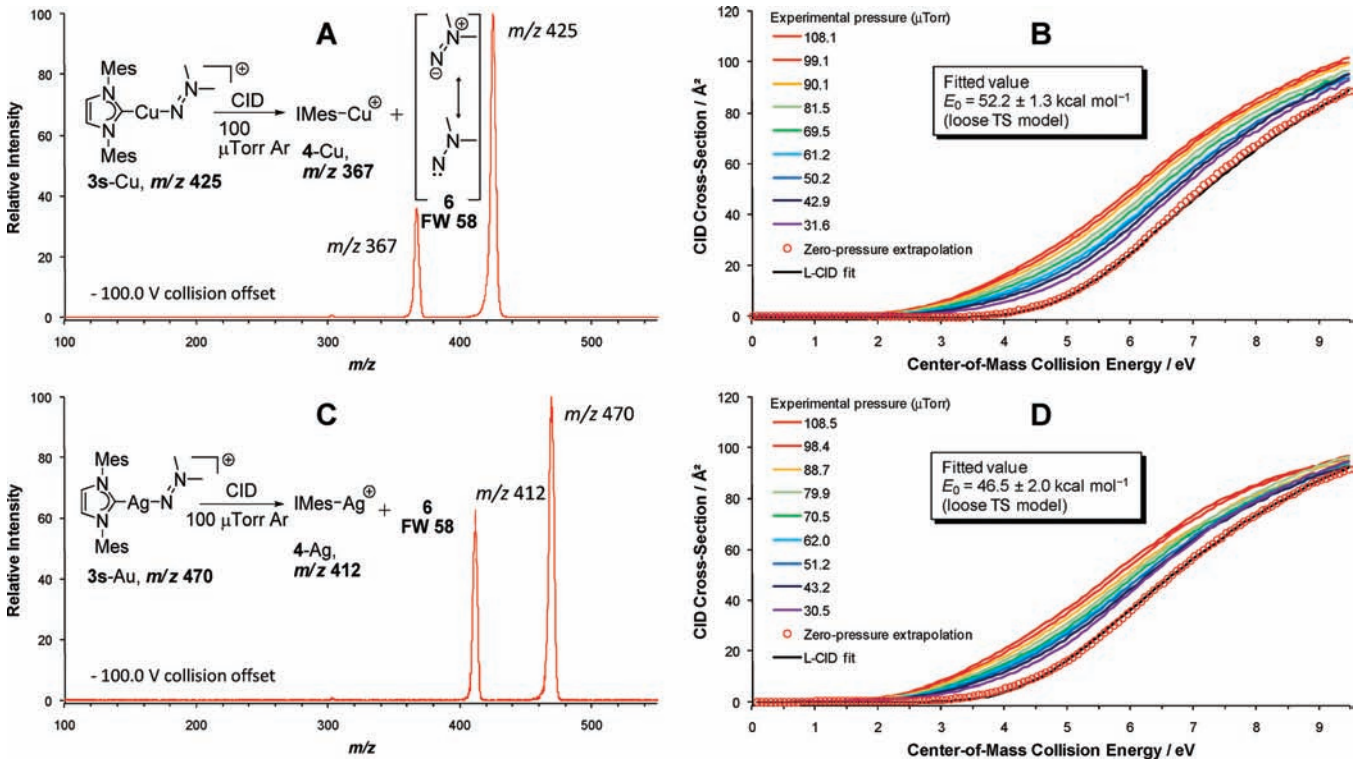

Figure 2. (Left) Daughter-ion mass spectra obtained after selection of cations **3s**-Cu (A) and **3s**-Ag (C) and CID with xenon in the octopole collision cell, demonstrating the breaking of the metal−nitrogen bond as the sole gas-phase reaction. (Right) Energy-resolved cross sections for loss of the aminonitrene fragment from **3s**-Cu (B) and **3s**-Ag (D) recorded at different Xe gas pressures, including linear extrapolations to zero pressure (red circles) and L-CID fits.

Table 1. Performance of the M06 Functional to Reproduce the Experimental Barriers[a]

	metal		
process: **3s** → **4** + **6s**	Cu	Ag	Au[13]
experiment	52.2 ± 1.3	46.5 ± 2.0	50.7 ± 1.6
calculated	60.6	45.0	58.7

[a] Energies are in kcal mol^{-1} and include zero-point energy corrections.

Table 2. BP86/TZP Energy Decomposition Analysis of the M−N Bond in Aminonitrene Complexes **3s** in kcal mol^{-1}

	Cu	Ag	Au
ΔE_{int}	−63.85	−48.20	−63.68
steric	−14.78	−10.91	−5.42
ΔE_{Pauli}	92.67	76.70	116.61
ΔV_{elstat}[a]	−107.45 [68.6]	−87.61 [70.1]	−122.03 [67.7]
ΔE_{oi}[a]	−49.07 [31.4]	−37.29 [29.9]	−58.26 [32.3]
A′[b]	−35.59 (72.5)	−30.22 (81.0)	−47.14 (80.9)
A″[b]	−13.48 (27.5)	−7.07 (19.0)	−11.12 (19.1)
ΔE_{prep}	1.73	1.23	1.50
4-M	0.68	0.28	0.15
6s	1.05	0.95	1.35
ΔE_{Net}	−62.12	−46.97	−62.18
q(**6s**)[c]	0.067	0.128	0.147
M−N (Å)	1.851	2.108	2.056
M−C (Å)	1.886	2.086	2.031

[a] Percentage of total stabilization in square brackets. [b] Percentage of ΔE_{oi} in parentheses. [c] Hirshfeld charge on the nitrene fragment.

in observed bonding strength in the order Au ≈ Cu > Ag and to obtain a more detailed description of the electronic structure of these species. Table 2 presents the results at the BP86/TZP level of theory. In analogy with reported bonding analyses of other coinage-metal complexes,[40] about 70% of the total stabilization comes from the electrostatic interaction V_{elstat}. The trend in bond strength results mainly from the total orbital interactions ΔE_{oi}, which decrease from −58.26 kcal mol^{-1} for Au to −49.07 kcal mol^{-1} for Cu and −37.29 kcal mol^{-1} for Ag, with a slight moderation from the overall steric interactions (Cu: −14.78, Ag: −10.91, Au: −5.42 kcal mol^{-1}).

We used C_s-symmetric structures to further decompose the orbital interactions into symmetrical (A′) and antisymmetrical (A″) contributions, which correspond to σ-type donation from the aminonitrene to the metal and π-back-bonding from a filled metal d orbital to the aminonitrene, respectively. Notably, for both **3s**-Ag and **3s**-Au the σ donation constitutes 81% of the total orbital interactions versus only 72.5% for **3s**-Cu (Table 2). Next, we identified the fragment orbitals that are primarily responsible for the bonding, i.e. those that are net electron donating or accepting, and compared their shapes, overlaps, and energy levels in the field of the total complex (Scheme 2).[29]

The uncoordinated aminonitrene **6s** has considerable N−N double-bond character as shown by its one-but-highest occupied molecular orbital (HOMO−1) in the middle of Scheme 2, resulting in a rather dipolar structure with a calculated dipole moment of 3.92 D. One lone electron pair on the terminal

(40) (a) Nemcsok, D.; Wichmann, K.; Frenking, G. *Organometallics* **2004**, *23*, 3640–3646. (b) Nechaev, M. S.; Rayón, V. M.; Frenking, G. *J. Phys. Chem. A* **2004**, *108*, 3134–3142. (c) Boehme, C.; Frenking, G. *Organometallics* **1998**, *17*, 5801–5809. (d) Hu, X.; Castro-Rodriguez, I.; Olsen, K.; Meyer, K. *Organometallics* **2004**, *23*, 755–764. (e) Tai, H.-C.; Krossing, I.; Seth, M.; Deubel, D. V. *Organometallics* **2004**, *23*, 2343–2349. (f) Kahlal, S.; Saillard, J.-Y.; Hamon, J.-R.; Manzur, C.; Carrillo, D. *New J. Chem.* **2001**, *25*, 231–242. (g) Hertwig, R. H.; Koch, W.; Schröder, D.; Schwarz, H.; Hrušák, J.; Schwerdtfeger, P. *J. Phys. Chem.* **1996**, *100*, 12253–12260. (h) Cundari, T. R. *Chem. Rev.* **2000**, *100*, 807–818.

Scheme 2. Primary Fragment Orbitals Involved in the M−N Bonding, with Indicated Energy Gaps ΔE_g (in the field of the total complex) in eV and Orbital Overlaps *S*

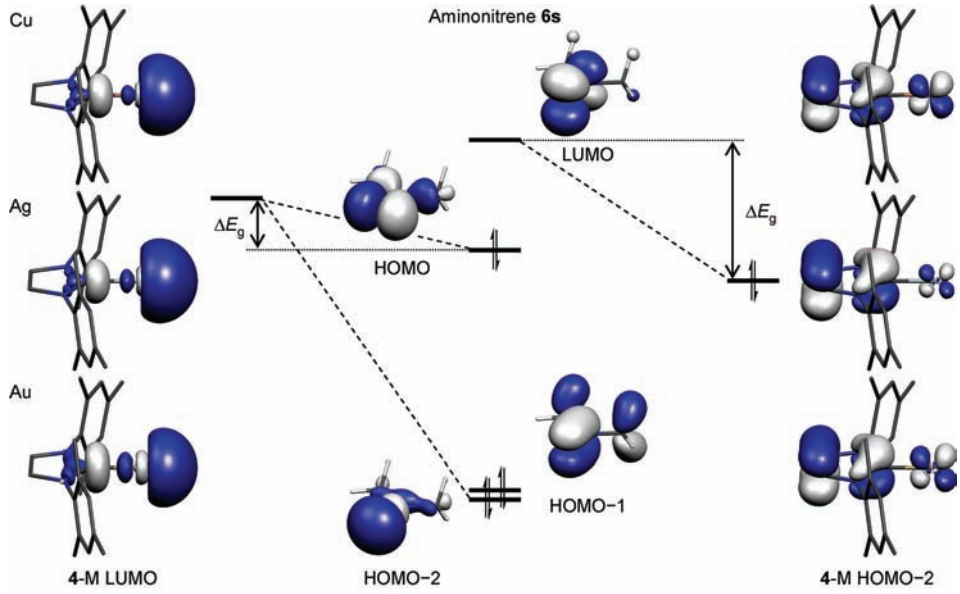

	A′ − σ Donation		A″ − π Backbonding	
	ΔE_g	$S \times 10^{-2}$	ΔE_g	$S \times 10^{-2}$
Cu	−1.01	21.7	2.60	6.22
Ag	0.51	22.2	2.78	2.71
Au	0.27	23.4	2.59	4.90

nitrogen atom is opposite the bond in an sp-hybrid orbital (HOMO−2) whereas the second lone pair is mostly localized in the remaining N-*p* orbital (HOMO). These two fragment orbitals interact mainly with the metal-centered lowest unoccupied orbital (LUMO, Scheme 2, left) of **4**-M and rehybridize to the sp^2-type σ-donor pair and lone pair inferred from the bent M−N−N arrangement in the total complexes **3s**-M. For all three metals, the shapes and overlaps *S* of the A′-symmetric fragment orbitals are comparable (Scheme 2). The trend in σ-donor strength of Au > Cu > Ag (Table 2) is due to the contraction and consequent lowering in energy of the sp-type LUMO of **4**-Au by relativistic effects.[31] As a result, this LUMO is only 0.27 eV above the nitrene HOMO for gold to give a more stabilizing interaction than for silver, where the energy gap ΔE_g is 0.51 eV. In contrast, the LUMO of **4**-Cu is calculated to be as much as 1.01 eV *below* the nitrene HOMO, so that the better interaction with the HOMO−2 leads to an intermediate stabilization.

For the π back-bonding the energy gaps ΔE_g are much larger and are relatively similar for all three metals. Instead, the trend Cu > Au > Ag is caused by marked differences in the shape of the HOMO−2 of **4**-M and therefore its overlap *S* with the nitrene LUMO (Scheme 2, right). The **4**-M HOMO−2 embodies the antibonding interaction of the *N*-heterocyclic carbene π-system with the metal d_{yz} orbital (where the M−N bond is along the *z*-axis). The d_{yz} contribution is largest for copper and smallest for silver, reflecting that the Ag-d orbitals are lower in energy than those of Cu, whereas for gold the relativistically contracted s and p core orbitals shield the nucleus more so that the valence d orbitals are at an intermediate energy level.[31]

DFT Calculations on Isomerization Pathways. Species **3s** are prepared using relatively high tube lens voltages (around 100 V), that is, offering an energy in excess of that required to break the N−P bond in **2**. Given the known propensity of aminonitrenes to isomerize,[37,41] we were motivated to confirm the identity of thus prepared ion currents **3s**-M. However, in contrast to gold carbenes,[12] we found no characteristic reactivity that would allow unambiguous identification of the metal-bound aminonitrenes. Collision of **3s**-Au with either butane or 1-butene afforded identical dissociation profiles, thus confirming the absence of any aziridination activity, which in turn can be explained by strong resonance stabilization present in the aminonitrene moiety.[13] Therefore, we conducted extensive DFT calculations to determine the barrier heights for conceivable isomerization pathways for species **3s**. In addition, the frequency analyses of the calculated isomeric species served for comparison with the experimental IR spectra (*vide infra*).

Scheme 3 presents the potential energy surface for the isomerization of metal-bound aminonitrenes **3s**-M to azomethanes **8** or **10** and to formaldehyde hydrazone **13**. Additionally, we located the transition states for intramolecular C−H insertion leading to diaziridines **14**. Although such processes are expected

(41) (a) Hinsberg, W. D., III; Dervan, P. B. *J. Am. Chem. Soc.* **1979**, *101*, 6142–6144. (b) Schultz, P. G.; Dervan, P. B. *J. Am. Chem. Soc.* **1980**, *102*, 878–880. (c) Hinsberg, W. D., III; Schultz, P. G.; Dervan, P. B. *J. Am. Chem. Soc.* **1982**, *104*, 766–773. (d) McIntyre, D. K.; Dervan, P. B. *J. Am. Chem. Soc.* **1982**, *104*, 6466–6468.

Scheme 3. Computed Energy Profile for the Isomerizations of **3s**-M[a]

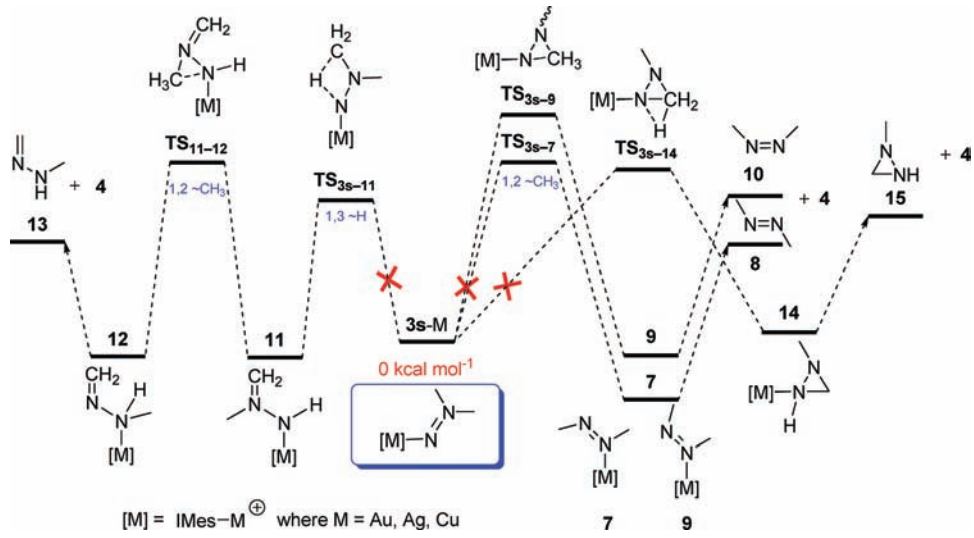

[a] The crossed-out processes involve barriers that should be inaccessibly high in energy under the experimental conditions (see text).

Scheme 4. Alternative Pathways to Furnish Formaldehyde Hydrazone **13**

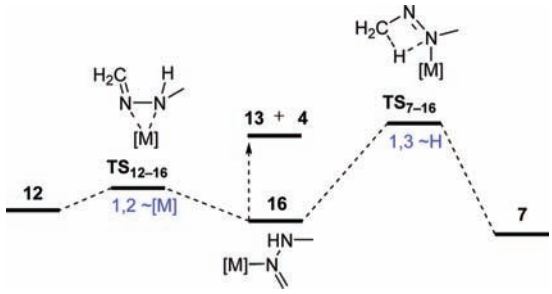

for metal nitrenes[36,42,43] and acceptor-substituted aminonitrenes,[44] to the best of our knowledge these were not reported for simple alkyl aminonitrenes. Alternatively, hydrazone **13** might be eliminated from species **16**, which could be formed via two pathways as shown in Scheme 4. Table 3 lists the M06 relative energies for all intermediates and transition states involved in Schemes 3 and 4.

As apparent from Table 3, the rearrangement of complexes **3s** to hydrazone species **11** is the pathway involving the lowest barrier (**TS$_{3s-11}$**-M, Cu: 57.4, Ag: 56.9, Au: 57.6 kcal mol^{-1}). The measured N−P bond strength in **2**-Au amounts to 45.0 ± 2.7 kcal mol^{-1},[13] which is expected to be similar for the analogous copper and silver adducts (see also the Supporting Information). This means that an activation energy of over 100 kcal mol^{-1} would be required for the subsequent occurrence of any of the rearrangements presented in Scheme 3. Such a large amount of energy should not be available under the experimental conditions applied. To get experimental confirmation of this inference, gas-phase IR spectroscopy[16] was conducted as discussed below.

Table 3. M06 Relative Energies for the Rearrangement of Metalloaminonitrenes **3s** into Azomethane (**8**, **10**), Hydrazone (**13**), or Diaziridine (**15**) Derivatives and Their Bonding Energies to the Metal Fragment (in kcal mol^{-1}, including zero-point energy corrections)

metal	TS$_{3s-7}$	7 (*trans*)	8 + 4	TS$_{3s-9}$	9 (*cis*)	10 + 4
Cu	64.8	−10.2	41.5	73.3	−2.7	50.1
Ag	63.0	−12.5	27.5	70.6	−4.7	36.1
Au	63.8	−10.4	40.3	72.7	−3.0	48.9

metal	TS$_{3s-11}$	11	TS$_{11-12}$	12	13 + 4
Cu	57.4	−2.4	66.1	−3.3	42.3
Ag	56.9	−2.4	65.6	−4.9	28.3
Au	57.6	−0.8	67.4	−1.7	41.1

metal	TS$_{3s-14}$	14	15 + 4	TS$_{12-16}$	16	TS$_{7-16}$
Cu	67.6	5.6	54.9	3.8	−8.9	49.4
Ag	67.0	4.0	40.9	−1.1	−10.7	47.6
Au	68.0	6.5	53.7	9.0	−8.5	50.0

IR−UV Double Resonance Spectroscopy. Gas-phase UV and IR spectra of all three species **3s**-M were recorded at $T \approx 10$ K in a 22-pole ion trap. The UV spectra (not shown here) appeared to be broad and featureless, spanning from 30500 cm^{-1} to at least 32800 cm^{-1} for **3s**-Au, for example. Such broad UV spectra usually inhibit the use of the IR−UV depletion scheme for vibrational spectroscopy of polyatomics. Indeed, no depletion of UV laser-induced photofragmentation was detected at various wavelengths across the measured part of the UV spectra for all three species studied here. In contrast, IR absorption *increased* the subsequent UV photofragmentation of the **3s**-M species when the UV laser frequency was tuned to the low-wavenumber edge of the UV absorption band. The nature of this gain must be an additional broadening and/or red shift of the spectra of vibrationally warm ions relative to those of the cold ones. Both

(42) (a) Berry, J. F. *Comments Inorg. Chem.* **2009**, *30*, 28–66. (b) Sharp, P. S. *Comments Inorg. Chem.* **1999**, *21*, 85–114. (c) Cundari, T. R. *J. Am. Chem. Soc.* **1992**, *114*, 7879–7888.
(43) (a) Cui, Y.; He, C. *Angew. Chem., Int. Ed.* **2004**, *43*, 4210–4212. (b) Cui, Y.; He, C. *J. Am. Chem. Soc.* **2003**, *125*, 16202–16203. (c) Li, Z.; Capretto, D. A.; Rahaman, R.; He, C. *Angew. Chem., Int. Ed.* **2007**, *46*, 5184–5186. (d) Li, Z.; Ding, X.; He, C. *J. Org. Chem.* **2006**, *71*, 5876–5880. (e) Badiei, Y. M.; Krishnaswamy, A.; Melzer, M. M.; Warren, T. H. *J. Am. Chem. Soc.* **2006**, *128*, 15056–15057. (f) Badiei, Y. M.; Dinescu, A.; Dai, X.; Palomino, R. M.; Heinemann, F. W.; Cundari, T. R.; Warren, T. H. *Angew. Chem., Int. Ed.* **2008**, *47*, 9961–9964.
(44) (a) Anderson, D. J.; Gilchrist, T. L.; Horwell, D. C.; Rees, C. W. *Chem. Commun.* **1969**, 146–147. (b) Zibinsky, M.; Stewart, T.; Prakash, G. K. S.; Kuznetsov, M. A. *Eur. J. Org. Chem.* **2009**, 3635–3642. (c) Zibinsky, M.; Butkevich, A. N.; Kuznetsov, M. A. *Tetrahedron Lett.* **2008**, *49*, 5505–5507.

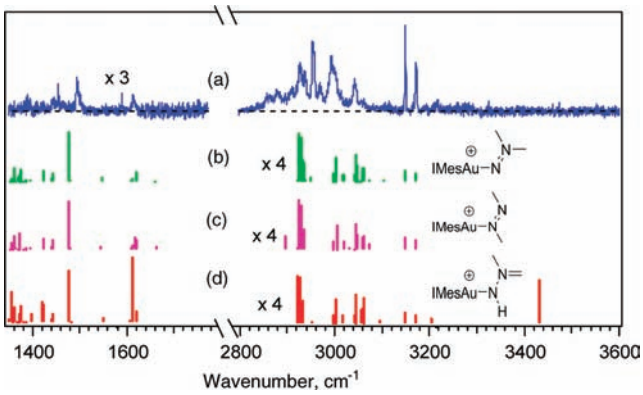

Figure 3. Experimental double-resonance photodissociation gain spectrum (a) and calculated vibrational spectra of **3s**-Au (b), **7**-Au (c), and **11**-Au (d).[45] The measured trace reflects the increase of the UV photodissociation yield for the $m/z = 501$ channel upon IR pre-excitation of cold sample ions; the UV laser frequency was fixed at 31790 cm^{-1}. The calculated frequencies are scaled by a factor of 0.9691 to account for anharmonicity of the vibrations.

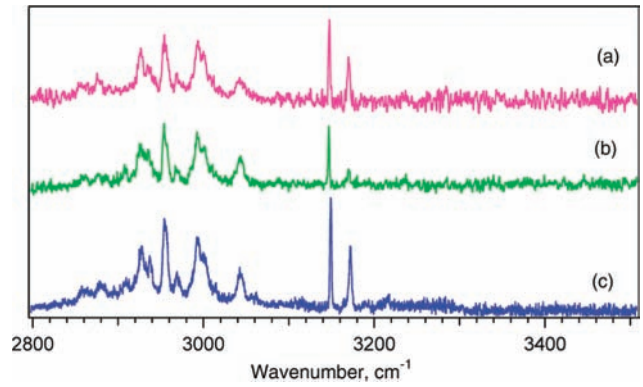

Figure 4. Experimental IR/UV photodissociation gain spectra of **3s**-Cu (a), **3s**-Ag (b), and **3s**-Au (c) cations. The UV laser frequency was fixed at 31230, 35690, and 31790 cm^{-1} for the Cu-, Ag-, and Au-containing species, respectively.

effects would result in an increased absorption near the low-frequency edge of the UV spectra. The exact UV wavelength is thus not critical and is a matter of compromise between the gain factor and the absolute photodissociation yield.

The left part of Figure 3 presents the IR spectrum of IMes-supported Au dimethylaminonitrene cation **3s**-Au in the 6-μm region (1350−1800 cm^{-1}) as measured by fixing the UV laser at 31790 cm^{-1} and detecting the $IMesAu^+$ fragment ($m/z = 501$). At least four prominent peaks appear in this region, which correspond to skeletal vibrations of the mesityl groups and imidazolium ring according to our frequency calculations. Some weaker transitions may be hidden by the noise in this part of the measured spectrum. The limited number of resolved peaks in this region does not allow unambiguous assignment of the studied species to one of the calculated structures (Figure 3 left, b−d).

The 3-μm region (2800−3500 cm^{-1}) appears to be more informative (Figure 3, right). The doubled photon energy and 4−5 times higher OPO pulse energy in this region as compared to the 6-μm range result in an 8 times higher gain factor, allowing the detection of many spectral features. The incompletely resolved broad band in the region of 2850−3050 cm^{-1} belongs to the skeletal C−H stretch vibrations. The two separate peaks at 3149 and 3171.8 cm^{-1} with linewidths of 2.2 and 3 cm^{-1} should arise from highly isolated C−H stretches. Indeed, vibrational frequency calculations suggest that these transitions belong to the antisymmetric and symmetric C−H stretch vibrations of the imidazolium moiety, respectively. An important feature of the measured spectrum that unambiguously constrains selection of possible structures is the lack of any detectable absorption above ∼3180 cm^{-1}. Our calculations suggest that species such as **11**-Au should feature an N−H stretch band above ∼3200 cm^{-1},[45] and therefore we can rule out these isomers based on the spectroscopic observations.

Figure 4 compares the 3-μm region of the experimental IR spectrum of the IMes-Au aminonitrene intermediate (Figure 3a) with those of the analogous IMes-Cu and IMes-Ag complexes. The latter two spectra have been measured with the UV laser wavenumber fixed at 31230 cm^{-1} and 35690 cm^{-1} and by detecting fragments with $m/z = 367$ Da and $m/z = 412$ Da (corresponding to loss of the aminonitrene group) for the copper and silver complex, respectively. The IR spectra of all three species are very similar and exhibit about the same maximum gain of ∼2. The only detectable spectral difference is a minor shift in the positions of the two highest-frequency peaks: for **3s**-Cu these are located at 3147.6 and 3170 cm^{-1} with linewidths of 2.2 and 3.7 cm^{-1}, respectively, whereas for **3s**-Ag the peaks appear at 3146.7 and 3169.9 cm^{-1} with linewidths of 1.9 and 2.9 cm^{-1}, respectively. The positions and sharp linewidths of these two peaks in all three spectra imply their assignment as the aforementioned imidazolium C−H stretches rather than as N−H stretch vibrations. Moreover, the high similarity between the three IR spectra suggests that the generated species should be structurally homologous; and hence, any NH-containing isomeric structures are unequivocally ruled out.

The experimental IR spectra do not allow us to directly assign the experimental species to structure **3s**-M and rule out azomethane adducts **7** or **9** (Scheme 4, see also spectra a−c in Figure 3), because of the high similarity of their computed IR spectra. However, the calculated barrier heights for formation of adducts **7** and **9** are higher than those leading to hydrazone **11** or diazirine **14** and, knowing from the experiments that no N−H containing species have been formed, one should reject possible isomerization to **7** and **9** as well. We thus are confident in assigning the gold, silver, and copper adducts appearing in our experiments to the species **3s**-M, although some finer details of their structures may differ from the calculated ones.

Discussion

A number of trend studies of d^{10} metal complexes with olefins, aryls, and alkynes have been reported recently.[46,47] The accumulated experimental and computational[40] data on the

(45) See Supporting Information for calculated IR spectra of all conceivable isomeric species.

(46) (a) Dias, H. V. R.; Lovely, C. J. *Chem. Rev.* **2008**, *108*, 3223–3238. (b) Dias, H. V. R.; Wu, J. *Eur. J. Inorg. Chem.* **2008**, 509–522. (c) Dias, H. V. R.; Flores, J. A.; Wu, J.; Kroll, P. *J. Am. Chem. Soc.* **2009**, *131*, 11249–11255. (d) Kazi, A. B.; Dias, H. V. R.; Tekarli, S. M.; Morello, G. R.; Cundari, T. R. *Organometallics* **2009**, *28*, 1826–1831. (e) Pérez-Galán, P.; Delpont, N.; Herrero-Gómez, E.; Maseras, F.; Echavarren, A. M. *Chem.—Eur. J.* **2010**, *16*, 5324–5332. (f) Shapiro, N. D.; Toste, F. D. *Proc. Natl. Acad. Sci. U.S.A.* **2008**, *105*, 2779–2782. (g) For a related study of Group 11 carbonyl complexes, see: Antes, I.; Dapprich, S.; Frenking, G.; Schwerdtfeger, P. *Inorg. Chem.* **1996**, *35*, 2089–2096.

(47) A recent computational study on gold(I) alkene and alkyne π complexes suggests a large amount of π back-donation from gold: Salvi, N.; Belpassi, L.; Tarantelli, F. *Chem.—Eur. J.* **2010**, *16*, 7231–7240.

Scheme 5. Resonance Structures for Aminonitrenes **3s**-M and One of Fürstner's Gold-Stabilized Carbocations

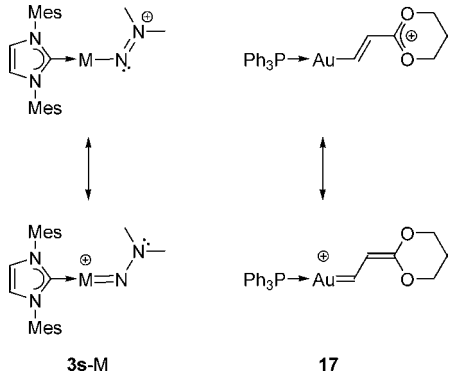

binding of the π-system in those cationic complexes revealed the bond strengths to change in the order Au > Cu > Ag, in agreement with the carbophilic character (a phenomenological designation) of gold widely exploited in catalysis.[11] As apparent from our bonding energy decomposition analyses, this effect can be explained by the relativistic contraction of the accepting 6s orbital on gold, which decreases the HOMO−LUMO gap with the ligand donor orbitals. In turn, stronger metal−ligand bonds in Cu complexes as compared to Ag are attributed to the greater back-donation from 3d orbitals on copper to vacant ligand orbitals.[46a,b]

On the other hand, literature data on the bonding of cationic coinage metals to σ-donating and π-accepting ligands such as carbenes or nitrenes are scarce, and in the case of gold, resulted in a certain controversy.[48] Namely, Fürstner has suggested that Au(I) carbene intermediates in cycloisomerizations of enynes are more consistently described as gold-stabilized carbocations,[48a] which might lack significant π-back-bonding due to a mismatch in orbital size.[48b] Subsequently, in an experimental and theoretical study Toste and Goddard argued that the character of these intermediates lies on a continuum and is determined by both the substitution and the supporting ligand.[48c] The aminonitrenes **3s**-M can be considered as isostructural to Fürstner's gold-stabilized carbocations (e.g., **17** in Scheme 5), having an electron-donating amino functionality as compared to isoelectronic alkoxy groups. Yet, our bonding analyses show considerable π-back-bonding in **3s**-Au and a moderate charge transfer from $IMesAu^+$ as indicated by a Hirshfeld charge[30] of +0.15 on the aminonitrene fragment (Table 2).

We also wish to point out that transition state $\mathbf{TS_{3s\text{-}14}}$, which was located for the intramolecular C−H insertion of metal-bound aminonitrenes **3s**, appears to be energetically nearly metal-independent, as are the corresponding methyl shifts (Scheme 3), and in fact, transition states $\mathbf{TS_{3s\text{-}14}}$ and $\mathbf{TS_{3s\text{-}7}}$ are also geometrically very similar for M = Cu, Ag, Au. The transition metal does make a difference, however, when a switching of coordination occurs as in $\mathbf{TS_{12-16}}$ or in any of the dissociation processes (Scheme 3). In these cases, our M06 calculations predict the same bond strength order as we have experimentally observed for the dissociation of **6s**: Cu ≈ Au > Ag.

(48) (a) Fürstner, A.; Morency, L. *Angew. Chem., Int. Ed.* **2008**, *47*, 5030–5033. (b) Seidel, G.; Mynott, R.; Fürstner, A. *Angew. Chem., Int. Ed.* **2009**, *48*, 2510–2513. (c) Benitez, D.; Shapiro, N. D.; Tkachouk, E.; Wang, Y.; Goddard, W. A., III; Toste, F. D. *Nat. Chem.* **2009**, *1*, 482–486.

Scheme 6. Proposed Rationale for the Formation of $IMesM(PPh_3)^+$ for M = Ag and Cu

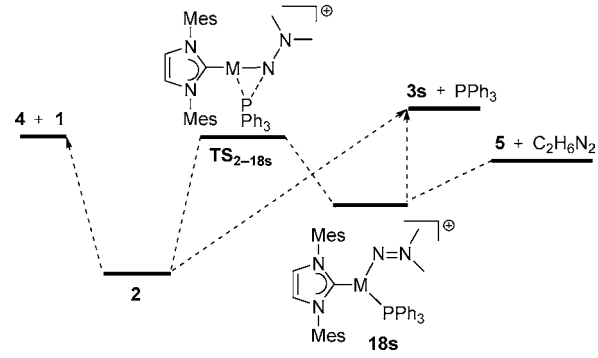

Lastly, we address the peculiar difference in the CID daughter channels of the parent phosphazene adducts **2s**. Alvarez and co-workers have studied the factors responsible for an increase of the coordination number in coinage metal complexes.[49] The strong preference for di-coordinated gold complexes was explained by the high deformation energy required to bend almost linear two-coordinate gold structures. Formation of species **5** most likely occurs via a tricoordinate aminonitrene intermediate **18s** that is connected to the starting phosphazene adduct **2** through a 1,2-PPh_3 shift (Scheme 6). The deformation energy will therefore destabilize transition state $\mathbf{TS_{2\text{-}18s}}$ for gold as compared to those for the copper and silver analogues, and this channel is therefore not observed for **2**-Au.

Conclusions

The combination of structure-sensitive, vibrationally resolved IR spectra with calculated spectra and barriers for conceivable isomerization pathways of Cu-, Ag-, or Au-bound aminonitrenes allows for a reliable structural assignment, from which bonding models in those complexes are explored with confidence. Threshold CID measurements provide the order of absolute binding energies of the dimethylaminonitrene fragment to isoleptic d^{10} Lewis acidic complexes to be Au ≈ Cu > Ag. Bonding analysis shows that relativistic effects for gold are responsible for the observed binding strength order and that a non-negligible fraction of the electron density from copper or gold is transferred to the aminonitrene fragment via π-back-donation. The latter has consequences for a much-discussed topic of a character of gold carbenoids, suggesting that the orbital size mismatch does not appear to be large enough to suppress the π-back-bonding interaction.

Acknowledgment. We acknowledge support of this work by the ETH Zürich, the EPF Lausanne and the Swiss National Science Foundation (Grants 20-120065 and 20-121810).

Supporting Information Available: Computational details, energies, geometries, reference mass spectra, experimental distribution of ion kinetic energies, as well as the energy-resolved collision-induced dissociation data and full reference 24. This material is available free of charge via the Internet at http://pubs.acs.org.

JA104649K

(49) Carvajal, M. A.; Novoa, J. J.; Alvarez, S. *J. Am. Chem. Soc.* **2004**, *126*, 1465–1477.